

Structure–Activity Relationship for Small Molecule Inhibitors of Nicotinamide *N*-Methyltransferase

Harshini Neelakantan,[†] Hua-Yu Wang,[‡] Virginia Vance,[†] Jonathan D. Hommel,[§] Stanton F. McHardy,[‡] and Stanley J. Watowich^{*,†,§}

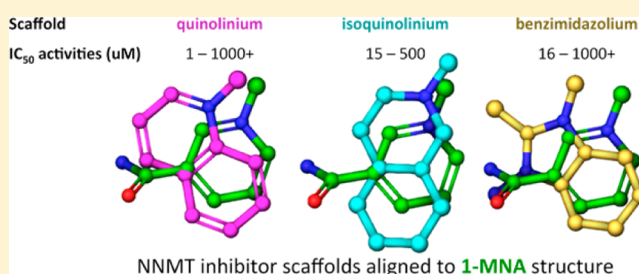
[†]Department of Biochemistry and Molecular Biology, University of Texas Medical Branch, Galveston, Texas 77550 United States

[‡]Department of Chemistry and Center for Innovative Drug Discovery, University of Texas at San Antonio, San Antonio, Texas 78249 United States

[§]Department of Pharmacology and Toxicology, University of Texas Medical Branch, Galveston, Texas 77550 United States

S Supporting Information

ABSTRACT: Nicotinamide *N*-methyltransferase (NNMT) is a fundamental cytosolic biotransforming enzyme that catalyzes the *N*-methylation of endogenous and exogenous xenobiotics. We have identified small molecule inhibitors of NNMT with >1000-fold range of activity and developed comprehensive structure–activity relationships (SARs) for NNMT inhibitors. Screening of *N*-methylated quinolinium, isoquinolinium, pyridinium, and benzimidazolium/benzothiazolium analogues resulted in the identification of quinoliniums as a promising scaffold with very low micromolar ($IC_{50} \sim 1 \mu M$) NNMT inhibition. Computer-based docking of inhibitors to the NNMT substrate (nicotinamide)-binding site produced a robust correlation between ligand–enzyme interaction docking scores and experimentally calculated IC_{50} values. Predicted binding orientation of the quinolinium analogues revealed selective binding to the NNMT substrate-binding site residues and essential chemical features driving protein–ligand intermolecular interactions and NNMT inhibition. The development of this new series of small molecule NNMT inhibitors direct the future design of lead drug-like inhibitors to treat several metabolic and chronic disease conditions characterized by abnormal NNMT activity.



INTRODUCTION

Nicotinamide *N*-methyltransferase (NNMT) is a cytosolic enzyme that catalyzes the transfer of methyl group from the cofactor *S*-(*S*'-adenosyl)-*L*-methionine (SAM) to substrates such as nicotinamide (NCA), pyridine, and related analogues (e.g., quinoline, isoquinoline, 1,2,3,4-tetrahydroisoquinoline¹), directly regulating the detoxification of endogenous and exogenous drugs/xenobiotics by the formation of methylated metabolic products (1-methyl nicotinamide [1-MNA], methylated pyridiniums, and methylated related analogues).² Given its primary metabolizing function, NNMT is predominantly expressed in the liver,^{3–5} but significant levels of the enzyme are also present in other tissues, including the adipose tissue, kidney, brain, lung, heart, and muscle.^{2,6} Enhanced expression and enzymatic activity of NNMT has been linked to a number of chronic disease conditions, making it a significant and relevant target for drug development. For example, several studies have demonstrated a causal relationship between increased NNMT expression and enhanced cell proliferation/progression in a variety of cancer cell lines with potential implications for NNMT as a biomarker for cancer prognosis and a target for anticancer therapeutic development.^{7–11} NNMT expression has also been reported to be upregulated in patients with Parkinson's disease, which is suggested to be

linked to the production of neurotoxins such as *N*-methylpyridinium ions that underlie neurodegeneration.^{12,13} Furthermore, studies in both animals^{14,15} and humans^{14,16,17} have shown that NNMT expression and activity was increased in obesity and related chronic metabolic conditions (e.g., type-2 diabetes). Knockdown of NNMT expression using an antisense oligonucleotide was reported to suppress body weight gain, reduce fat mass, and increase energy expenditure in mice fed a high fat diet.¹⁵ While the underlying molecular mechanisms that link decreased NNMT activity to increased adipocyte metabolism are not well understood, NNMT may modulate intracellular metabolite turnover in the methionine–homocysteine cycle and/or the nicotinamide adenine dinucleotide (NAD⁺) synthesis pathway critical for cellular energy expenditure.¹⁵ Therefore, targeted small molecule inhibitors of the NNMT could be significantly beneficial as molecular probes for mechanistic investigations and for the development of therapeutics to treat metabolic and chronic diseases that are characterized by abnormal NNMT activity.

SAM-dependent methyltransferases represent a major class of biotransforming enzymes that catalyze the methylation of

Received: March 15, 2017

Published: May 26, 2017

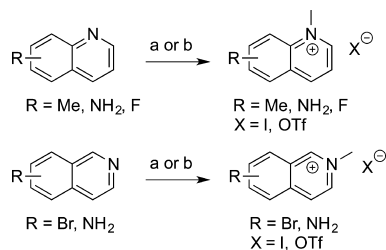
various substrates, including proteins, nucleic acids, and endogenous small molecules (e.g., intracellular metabolites) using the cofactor SAM as a universal methyl donor.^{18–20} Many inhibitors of SAM-dependent methyltransferases (e.g., the broad-spectrum methyltransferase inhibitor sinefungin, histone methyltransferase inhibitor EPZ-5676) mimic the chemical structure of SAM and interact with the SAM-binding site,^{21,22} thereby lacking selectivity for specific methyltransferase enzymes.²³ However, the recent determination of the structure of NNMT bound to the NCA substrate and SAH product²⁴ provide information that can be used to design selective and specific small molecule NNMT inhibitors.

On the basis of consistent observations of 1-MNA, the primary endogenous *N*-methylated product of NNMT, as an NNMT inhibitor in biochemical and pharmacological studies *in vitro* and *in vivo*,^{2,15} in the present study we explored the NNMT inhibitory activity of *N*-methylated heterocyclic small molecules containing several different aromatic scaffolds including quinoline, isoquinoline, pyridine, benzimidazole, and benzothiazole.^{1,25} Preliminary sets of *N*-methylated analogues for each of the chemical scaffolds were purchased from commercial suppliers and screened for NNMT inhibitory activity using purified recombinant protein. We expanded several promising chemical series to develop predictive structure–activity relationships (SARs) with emphasis on substitution effect on aryl ring and the N1 atom for each chemical series. Further, computer-based docking of inhibitors to the NNMT NCA substrate-binding site yielded a correlation between inhibitor–enzyme interaction docking scores and experimentally determined IC₅₀ values that served as a guiding tool to identify NNMT residues responsible for protein–ligand interactions and further generate binding hypotheses to design novel inhibitors with improved binding. The SAR described herein demonstrates significant promise for future exploration of the chemical space surrounding the template moieties to develop potent, selective, and drug-like NNMT inhibitors.

RESULTS AND DISCUSSION

Chemistry. The general approach to prepare the *N*1-methylated quinolinium and *N*2-methylated isoquinolinium salts was carried out as shown in Scheme 1. Commercially

Scheme 1. General Method for Synthesis of *N*-Methylated Quinolinium and Isoquinolinium Analogues^a



^aReagents and conditions: (a) MeI, IPA, 90 °C, 12 h; (b) MeOTf, toluene, 100 °C, 12 h.

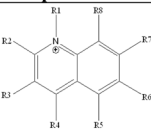
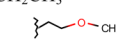
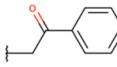
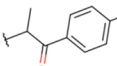
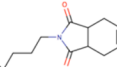
available and/or synthesized quinoline and isoquinoline with various substitution patterns were treated with iodomethane (MeI) in 2-propanol (IPA) or methyl trifluoromethanesulfonate (MeOTf) in toluene to give the corresponding analogues in good yields. Full details on the synthesis of the substituted

amino-quinoline and per-methylated quinoline intermediates/precursors are described in the Supporting Information.

Biological Evaluation of 1-Methylquinolinium (1-MQ) Analogues. To test the hypothesis that *N*-methylated quinolinium containing compounds function as NNMT inhibitors, we began by probing the NNMT inhibitory activity of 1-MQ (**1a**), which exhibited an IC₅₀ value of 12 μM (Table 1). On the basis of the activity exhibited by **1a**, we explored SAR for NNMT inhibition on the 1-MQ scaffold by testing 48 additional analogues (obtained either from commercial suppliers or synthesized in-house) using a modified HPLC-based biochemical assay.^{25,26} In the first series of compounds, we explored the inhibitory activities of monosubstituted 1-MQ with various polar/apolar substituents and different *N*1-substituted quinolinium analogues (**1b–z**; Table 1). Generally, small substituents such as methyl or amine groups were well tolerated in different substitution patterns on the 1-MQ ring with NNMT inhibitory activity in the low micromolar range (Table 1). Among all the monomethylated quinolinium analogues tested with various substitution patterns at C2–C8-positions of 1-MQ (**1b**, **1e**, **1i**, **1l**, **1n**, **1r**, and **1t**; Table 1), a methyl substituent at the C8-position (**1t**) gave the most significant improvement in inhibition (6.7-fold lower IC₅₀ value, IC₅₀ = 1.8 μM) as compared to the parent compound 1-MQ (**1a**). While a methyl substituent at the C3-position also exhibited low micromolar NNMT inhibition (**1e**, IC₅₀ = 4.1 μM; Table 1), an amino substitution at the same position further improved the IC₅₀ value to 2.9 μM (**1d**), suggesting relatively favorable interactions between the NNMT residues and the C3-amino substitution. To further explore the favorable nature of polar groups at the C3-position, we tested analogues **1f–h**; analogue **1f** with a C3-methylamino substitution and analogue **1g** with a cyano substituent at the C3-position had ~3-fold and ~8-fold higher IC₅₀ values, respectively, relative to compound **1d**. Importantly, analogue **1h** with a bulky phenyl ring at the C3-position had significantly reduced inhibitory activity (IC₅₀ > 1 mM). Taken together, the data suggests that potentially favorable interactions can be imparted by small polar group substituents such as an amine, while unfavorable steric interactions occur when large chemical groups occupy the C3-position of the 1-MQ scaffold.

To further explore 1-MQ scaffold positions that could form favorable hydrogen-bonding interactions with NNMT binding site residues to improve inhibitory activity, a systematic SAR was conducted among different amino-quinolinium derivatives (**1c**, **1d**, **1j**, **1k**, **1o**, **1q**; Table 1). Many of the 1-MQ analogues with amino pharmacophores (e.g., **1c**, **1k**, **1q**) demonstrated excellent inhibitory activities that were comparable to **1d** (IC₅₀ = 2.9 μM); the exceptions were analogues **1j** (C4-amino substituent) and **1o** (C6-amino substituent) that exhibited ~4-fold and ~10-fold reduction in activity (IC₅₀ = 11 μM and 34 μM), respectively, compared to **1d**. An amino substitution at the C5-position (**1k**) produced potent NNMT inhibition (IC₅₀ = 1.2 μM) with 10- and 2.4-fold lower IC₅₀ values compared to **1a** and **1d**, respectively (Figure 1; Table 1). This suggests that the polar amine group at the C5-position favors strong intermolecular interactions with the backbone serine residues in the NNMT substrate-binding site (refer to Molecular Docking discussion below). In contrast to amino substitutions, 1-MQ analogues with other polar substitutions such as hydroxyl (**1s** and **1u**) and methoxy (**1p**) showed significantly weaker NNMT inhibition activities compared to the parent compound **1a**. For example, a hydroxyl group substituent at the C7-

Table 1. NNMT Inhibitory Activity of 1-Methylquinolinium Scaffold Compounds with Single Positional Substitutions

Core/ Compound Name	R1	R2	R3	R4	R5	R6	R7	R8	NNMT Inhibition IC ₅₀ (μM) ^a
									
Quinoline									
1a (1-MQ)	CH ₃	H	H	H	H	H	H	H	12.1 ± 3.1
1b	CH ₃	CH ₃	H	H	H	H	H	H	21.03 ± 2.1 ^b
1c	CH ₃	NH ₂	H	H	H	H	H	H	6.3 ± 1.1 ^b
1d	CH ₃	H	NH ₂	H	H	H	H	H	2.9 ± 0.7 ^b
1e	CH ₃	H	CH ₃	H	H	H	H	H	6.9 ± 3.01 ^b
1f	CH ₃	H	NHCH ₃	H	H	H	H	H	9.9 ± 3.4 ^b
1g	CH ₃	H	CN	H	H	H	H	H	23.8 ± 5.6
1h	CH ₃	H	NHPh	H	H	H	H	H	>1000 ^b
1i	CH ₃	H	H	CH ₃	H	H	H	H	7.5 ± 2.2
1j	CH ₃	H	H	NH ₂	H	H	H	H	11.4 ± 2.1 ^b
1k	CH ₃	H	H	H	NH ₂	H	H	H	1.2 ± 0.1 ^b
1l	CH ₃	H	H	H	CH ₃	H	H	H	4.6 ± 1.8 ^b
1m	CH ₃	H	H	H	H	F	H	H	5.7 ± 1.8 ^b
1n	CH ₃	H	H	H	H	CH ₃	H	H	13.1 ± 5.1
1o	CH ₃	H	H	H	H	NH ₂	H	H	34.4 ± 9.6 ^b
1p	CH ₃	H	H	H	H	OCH ₃	H	H	119.9 ± 50.1
1q	CH ₃	H	H	H	H	H	NH ₂	H	2.6 ± 0.5 ^b
1r	CH ₃	H	H	H	H	H	CH ₃	H	12.01 ± 4.5 ^b
1s	CH ₃	H	H	H	H	H	OH	H	709.2 ± 178.9
1t	CH ₃	H	H	H	H	H	H	CH ₃	1.8 ± 0.5
1u	CH ₃	H	H	H	H	H	H	OH	95.2 ± 21.02
1v	CH ₂ CH ₃	H	H	H	H	H	H	H	27.1 ± 5.4
1w		H	H	H	H	H	H	H	>1000
1x		H	H	H	H	H	H	H	>1000
1y		H	H	H	H	H	H	H	>1000
1z		H	H	H	H	H	H	H	>1000

^aIC₅₀ values are represented at mean ± SD of duplicate or more measurements. ^bCompounds synthesized in-house.

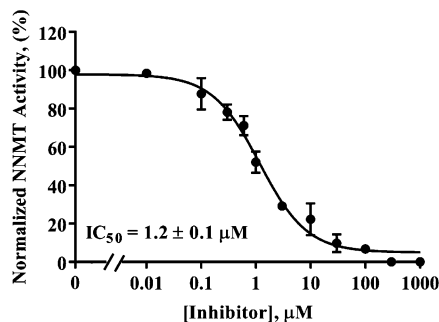
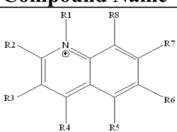
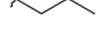
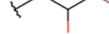


Figure 1. Normalized response curve for NNMT inhibitor **1k** (5-amino-1-methylquinolinium analogue). Data points represent average and standard deviation of normalized NNMT activity. Data points were normalized to no inhibitor condition (0 μM) within each experiment ($n = 5$). The goodness-of-fit R^2 between the fitted curves and data was 0.97.

position demonstrated ~50% inhibition of NNMT at nearly a millimolar concentration (**1s**, IC₅₀ = 709 μM), whereas the comparable amino-substituted analogue (**1q**) was a potent NNMT inhibitor (IC₅₀ = 2.6 μM). While this observation remains intriguing, it can be speculated based on our molecular docking analyses using predicted binding orientations of the analogues **1s** and **1q** that the N atom of the C7-amino forms a

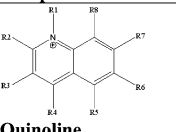
stronger hydrogen bond to the carbonyl oxygen side chain of Ser213 residue of NNMT, relative to the more repulsive hydrogen bond interaction between donor hydrogen atom of C7-hydroxyl and the Ser213 residue. Additionally, under the aqueous buffer reaction condition (pH 8.6) used in the current study, it is likely that the C7-hydroxy quinolinium analogue undergoes tautomerization into its dominant form (i.e., C7-oxo-dihydroquinolinium analogue), losing the charge on the N1 atom and significantly diminishing the overall binding within the NNMT substrate-binding site. Similarly, replacement of the methyl group (**1t**) by a polar hydroxyl substituent at the C8-position exhibited >50-fold lower IC₅₀ (**1u**, IC₅₀ = 95.2 μM) that may also be due to preferred ionization of the polar hydroxyl group in aqueous buffer, resulting in potential disruption of the tight binding within the apolar pocket of the NNMT binding site (refer to [Molecular Docking](#) discussion below). Lastly, we examined the relationship between quinolinium analogues containing N1 substitutions with varied steric and electronic properties (**1v–z**; [Table 1](#)) and NNMT inhibition. The results revealed that the activity of N1-substituted quinoliniums was inversely correlated with the size of the substituent. For example, N1-ethyl quinolinium analogue **1v** was an ~2-fold weaker inhibitor compared to 1-MQ (**1a**) and analogues with bulky substituents (**1w–z**) showed very poor inhibition (IC₅₀ > 1000 μM). These data

Table 2. NNMT Inhibitory Activity of 1-Methylquinolinium Scaffold Compounds with Dual Positional Substitutions^c

Core/ Compound Name	R1	R2	R3	R4	R5	R6	R7	R8	NNMT Inhibition IC ₅₀ (μM) ^a
									
Quinoline									
2a	CH ₂ CH ₃	H	H	CH ₃	H	H	H	H	8.7 ± 2.6
2b	CH ₂ CH ₃	H	H	H	H	H	H	CH ₃	3.1 ± 1.4
2c		H	H	CH ₃	H	H	H	H	33.5 ± 9.9
2d		H	H	H	H	H	H	OH	40.6 ± 13.01
2e		H	Br	H	H	H	H	H	>1000
2f	CH ₂ CH ₂ CH ₃	H	H	H	H	CH ₃	H	H	>1000
2g		H	H	H	H	Cl	H	H	>1000
2h		H	H	H	H	OH	H	H	>1000
2i		H	H	H	H	CH ₃	H	H	NI
2j	CH ₃	H	NH ₂	H	H	F	H	H	1.2 ± 0.2 ^b
2k	CH ₃	H	H	H	CF ₃	H	H	CH ₃	87.01 ± 26.1 ^b
2l	CH ₃	H	H	Cl	H	H	H	CF ₃	>1000 ^b
2m	CH ₃	NH ₂	NH ₂	H	H	H	H	H	2.8 ± 0.5 ^b
2n	CH ₃	CH ₃	H	H	H	H	H	CH ₃	15.9 ± 7.9 ^b
2o	CH ₃	CH ₃	H	H	H	CH ₃	H	H	>1000 ^b

^aIC₅₀ values are represented at mean ± SD of duplicate or more measurements. ^bCompounds synthesized in-house. ^cNI: No inhibition and area product peak was higher compared to control reaction.

Table 3. NNMT Inhibitory Activity of 1-Methylquinolinium Scaffold Compounds with Multipositional Substitutions

Core/ Compound Name	R1	R2	R3	R4	R5	R6	R7	R8	NNMT Inhibition IC ₅₀ (μM) ^a
									
Quinoline									
3a	CH ₂ CH ₃	H	H	CH ₃	H	F	H	H	3.6 ± 1.5
3b	CH ₂ CH ₃	H	H	CH ₃	H	CF ₃	H	H	>1000
3c	CH ₃	CH ₃	H	CH ₃	H	H	H	CH ₃	115.4 ± 41.01 ^b
3d	CH ₃	CH ₃	H	CH ₃	CH ₃	H	H	CH ₃	>1000 ^b
3e	CH ₃	CH ₃	H	CH ₃	H	CH ₃	H	CH ₃	>1000 ^b
3f	CH ₃	CH ₃	H	CH ₃	H	H	CH ₃	CH ₃	>1000 ^b
3g	CH ₃	CH ₃	H	CH ₃	F	H	H	CH ₃	94.6 ± 76.3 ^b
3h	CH ₃	CH ₃	H	CH ₃	H	H	F	CH ₃	109.2 ± 58.5 ^b

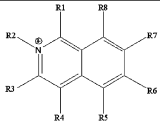
^aIC₅₀ values are represented at mean ± SD of duplicate or more measurements. ^bCompounds synthesized in-house.

suggest that small moieties such as methyl or ethyl groups directly adjacent to the N1 position may be crucial for maintaining potent NNMT inhibitory activity of the quinolinium scaffold.

To further develop an SAR model for the quinolinium scaffold, we next explored the activities of analogues with dual (2a–o; Table 2) and multipositional substitutions (3a–h; Table 3). Consistent with our previously observed inverse relationship between NNMT inhibition and N1 substituent size, N1-ethyl quinolinium analogues with C4- and C8-methyl substituents (2a,b; Table 2) showed lower activities compared to N1-methyl quinolinium congeners (1i and 1t; Table 1). Substituting a hydroxyethyl (2c) for an ethyl group (2a) at the

N1 position further reduced the activity by ~3.5-fold, reinforcing the observation that a smaller alkyl group (e.g., methyl) at the N1 position is valuable for maintaining good inhibitory potency. The relationship between NNMT inhibition and likely steric effects from N1 substitutions was further exemplified by analogues 2e–i, which displayed IC₅₀ values that either exceeded 1000 μM or showed no inhibition of NNMT, regardless of the pharmacophore (i.e., methyl, chloro, and hydroxyl groups) placed at the C6-position. Single-point SAR studies indicated that a C8-hydroxyl containing analogue (1u; Table 1) decreased the IC₅₀ value by ~50-fold relative to a more favorable methyl substituent (1t), while two-point SAR studies incorporating a hydroxyl group at the C8-position and a

Table 4. NNMT Inhibitory Activity of Compounds Containing 2-Methyl Isoquinolinium Scaffold

Core/ Compound Name	R1	R2	R3	R4	R5	R6	R7	R8	NNMT Inhibition IC ₅₀ (μM) ^a
 Isoquinoline									
4a	H	CH ₃	H	H	H	H	H	H	14.9 ± 6.1
4b	H	CH ₃	NH ₂	H	H	H	H	H	6.3 ± 2.7 ^b
4c	H	CH ₃	H	Br	H	H	H	H	30.3 ± 7.02 ^b
4d	H	CH ₃	H	H	H	NH ₂	H	H	29.9 ± 9.1 ^b
4e	H	CH ₃	H	H	H	Br	H	H	505.7 ± 199.1 ^b
4f	H	CH ₃	H	H	H	H	NH ₂	H	39.4 ± 18.02 ^b

^aIC₅₀ values are represented at mean ± SD of duplicate or more measurements. ^bCompounds synthesized in-house.

relatively bulky C2-oxopropyl at the N1 position (**2d**) did not additively impair activity; instead, the IC₅₀ value for **2d** was ~2-fold lower relative to **1u**. This may imply that substitutions at C8-position combined with branched groups at the N1 position might alter the binding mode of the analogue and disrupt the steric-dependent inhibition pattern observed with bulky groups at the quinolinium N1 position.

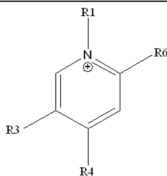
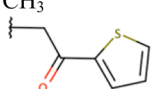
Interestingly, when a fluorine was added to the C6-position of the C3-amino-analogue (**1d**), we observed supra-additive effects on NNMT inhibition; the C3-amino C6-fluoro-1-MQ analogue (**2j**) had an IC₅₀ of 1.2 μM, which was ~2.5-fold more potent than the nonfluorinated derivative **1d** (IC₅₀ = 2.9 μM) and ~5-fold more potent than the C6-fluoro-1-MQ analogue (**1m**; IC₅₀ = 5.7 μM), highlighting the significance of both C3-amino and C6-fluoro substituents in improving activity. The improvement observed in NNMT inhibitory activity with the introduction of a fluorine substituent is consistent with the general observation that electron-withdrawing halogen groups such as fluorine may engage in multipolar interactions (e.g., orthogonal-type dipolar interaction with carbonyl groups in the binding pocket of a target protein), causing improvements in compound binding and affinity.^{27,28} Analogues with CF₃ substitutions have also been observed to form strong multipolar intermolecular interactions and improve binding affinities relative to the corresponding methyl derivatives.²⁹ CF₃ substituents were tested using several 1-MQ analogues; CF₃ substituent (**2k**; Table 2) placed at C5-position within the 1-MQ scaffold impaired activity relative to an analogue lacking this substituent (**1t**) and a CF₃ substituent at the C8-position (**2l**; Table 2) in addition to an impairing chloro substituent at the C4-position significantly deteriorated the activity of the compound. Further, we tested for other potentially synergistic effects by screening dual-substituent 1-MQ analogues containing numerous small apolar and amino pharmacophores. We found that the C2,3-diamino-1-MQ analogue **2m** showed inhibitory activity (IC₅₀ = 2.8 μM; Table 2) that was similar to the C3-amino 1-MQ analogue **1d** (IC₅₀ = 2.9 μM; Table 1) without additive improvements, reinforcing the observation that an amino-substituent at the C3-position is an important feature among 1-MQ analogues to maintain potent inhibitory activity. Similarly, other dimethyl substitutions in analogues (**2n–o**; Table 2) did not cause synergistic improvements in compound activity compared to the corresponding mono-methyl substitutions (**1b**, **1n**, **1t**; Table 1) but instead rendered the dimethyl quinolinium compounds as poor inhibitors of NNMT (5–50-fold higher IC₅₀ values, **2n–o**; Table 2).

In our studies of the activity of multipositionally substituted N1-quinoliniums, a C6-fluorinated analogue **3a** (IC₅₀ = 3.6 μM; Table 3) showed a ~2.5-fold increase in NNMT inhibitory activity compared to the nonfluorinated derivative **2a** (IC₅₀ = 8.7 μM; Table 2), consistent with earlier observations that C6-fluoro substitution positively impacts quinolinium inhibitory activity. Substitution of the C6-fluoro of analogue **3a** to a C6-trifluoromethyl group (**3b**) resulted in a significant loss of compound inhibitory activity (IC₅₀ > 1000 μM), comparable to the drastic reductions in NNMT inhibition observed when CF₃ substituents were incorporated into the quinolinium scaffold (analogues **2k–l**; Table 2).

General synthetic approaches were applied to improve the lipophilicity and drug-like properties (e.g., permeability) of this class of quinolinium-based NNMT inhibitors, in which the lipophilicity was evaluated in silico by measuring the calculated logarithmic form of the partition coefficient using ChemAxon software.³⁰ To this end, we tested several per-methylated quinolinium analogues with methyl substituents at multiple ring positions (C2–C8). Similar to the results obtained with dimethyl-substituted analogues, the addition of multiple methyl substituents largely decreased the ability of the analogues to inhibit NNMT (**3c–f**; Table 3). A C2,C4,C8-trimethyl-analogue **3c** showed ~5–64-fold lower inhibitory activity (IC₅₀ = 115.4 μM) as compared to monomethylated analogues such as **1b** (IC₅₀ = 21 μM), **1h** (IC₅₀ = 7.5 μM), and **1q** (IC₅₀ = 1.8 μM). Graphical analysis of molecular docking simulations suggested that multimethylated 1-MQ analogues make intermolecular apolar contacts with several hydrophobic residues within the NNMT binding site that are likely detrimental to the overall binding energetics between the ligand and enzyme; this conclusion was supported by poor docking scores generated by Vina ligand docking program. Furthermore, unlike the activity improvements observed for 1-MQ analogues with C6-fluoro group substitutions (see compounds **1k**, **2j**, **3a**), the addition of a fluoro group to the C5 or C7 positions of a per-methylated quinolinium scaffold (**3c**) did not improve analogue inhibitory potency (**3g**, IC₅₀ = 94.6 μM; **3h**, IC₅₀ = 109.2 μM; Table 3), suggesting that the C6-position may be highly “fluorophilic” to promote dipole-type interactions within the NNMT substrate-binding site. However, additional analogues with positional fluoro substitutions within the 1-MQ scaffold need to be tested to confirm this hypothesis.

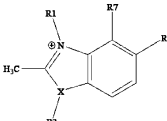
Biological Evaluation of N2-Methyl Isoquinolinium Analogues. Previous studies have shown that the isoquinoline

Table 5. NNMT Inhibitory Activity of Compounds Containing Pyridinium Scaffold

Core/ Compound Name	R1	R3	R4	R6	NNMT Inhibition IC ₅₀ (μM) ^a
					
Pyridine					
5a	CH ₃	CONH ₂	H	H	9.0 ± 0.6 ^b
5b	CH ₃	CONH ₂	CH ₃	CH ₃	11.8 ± 3.04
5c		CONH ₂	H	H	>1000

^aIC₅₀ values are represented at mean ± SD of duplicate or more measurements. ^b1-MNA (5a) is a reaction product of NNMT; IC₅₀ curve for 5a was determined using a fluorescence assay that utilizes quinoline as an NNMT substrate and monitors formation of 1-MQ.

Table 6. NNMT Inhibitory Activity of Compounds Containing Benzimidazolium/Benzothiazolium Scaffold

Core/ Compound Name	R1	R3	R6	R7	X	NNMT Inhibition IC ₅₀ (μM) ^a
						
Benzimidazol/ Benzothiazole						
6a	CH ₃	CH ₃	H	H	N	16.7 ± 6.4
6b	CH ₃	NH ₂	H	H	N	82.4 ± 17.4
6c	CH ₂ CH ₃	CH ₂ CH ₃	H	H	N	22.8 ± 7.8
6d	CH ₃	CH ₂ CH ₃	NH ₂	H	N	>1000
6e	CH ₂ CH ₃	-	CH ₃	H	S	>1000
6f	CH ₂ CH ₂ CH ₂ CH ₃	-	H	H	S	>1000

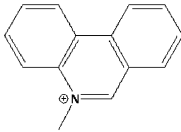
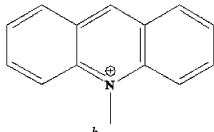
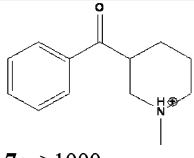
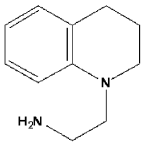
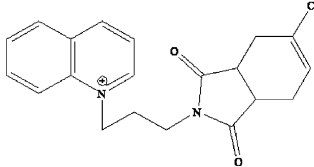
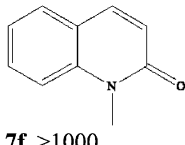
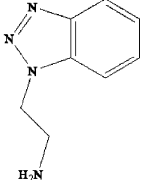
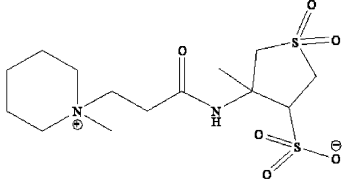
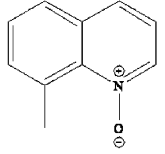
^aIC₅₀ values are represented at mean ± SD of duplicate or more measurements.

scaffold is amendable to the development of drug-like small molecule inhibitors.^{31,32} Because isoquinoline is also an NNMT substrate,^{1,25} we examined the NNMT inhibitory activities of a series of analogues designed around the N2-methyl isoquinolinium chemotype (Table 4). NNMT methylates isoquinoline to produce the reaction product N2-methyl isoquinolinium (4a),^{1,25} which inhibits NNMT with an IC₅₀ of 14.9 μM similar to that of 1-MQ (1a; IC₅₀ = 12.1 μM). Guided in part by the SAR established for the 1-MQ scaffold (Tables 1–3) and molecular docking calculations, we explored the activities of a small series of monosubstituted isoquinoline analogues (4b–f; Table 4). As summarized in Table 4, a C3-amino substituent (4b) improved compound activity ~2.4-fold (IC₅₀ = 6.3 μM) compared to the parent N2-methyl isoquinolinium (4a); the relative improvement in activity that resulted from adding a C3-amino group to the isoquinoline parent was smaller compared to the activity increase observed when the substitutional congener was added to the 1-MQ scaffold (1d, IC₅₀ = 2.9 μM). Instead, 4b had activity similar to analogue 1c (IC₅₀ = 6.3 μM); both analogues have an amino group adjacent to the N-methyl moiety, which could potentially shift the binding orientations of these analogues and disrupt some of the hydrophobic interactions within the NNMT substrate-binding site (a detailed discussion is presented in the Molecular Docking section below). Incorporation of a bromo group at the C4-

position (4c) or an amino group at the C6-position (4d) reduced the potency of these analogues by ~2-fold relative to the parent analogue (4a) while adding a bromo group at the C6-position (4e) significantly decreased analogue activity (IC₅₀ = 505.7 μM). In contrast to the 1-MQ chemotype (1a) where a C7-amino (1n) improved analogue potency by 5-fold, a comparable amino substitution pattern on the N2-methyl isoquinolinium scaffold decreased analogue potency by ~3-fold (4f; IC₅₀ = 39.4 μM). These observations are consistent with calculated changes to the binding orientations and intermolecular interactions between NNMT and N1-MQ and N2-methyl isoquinolinium analogues, respectively (refer to Molecular Docking discussion below).

Inhibitory Activities of 1-Methylpyridinium Analogues. 1-Methylnicotinamide (1-MNA; 5a) is the endogenous product of the NNMT catalyzed reaction and an established NNMT inhibitor.^{2,15} Using a recently developed sensitive fluorescence-based assay,³³ we determined the IC₅₀ of 1-MNA to be 9.0 μM (Table 5), which is comparable to the IC₅₀ value determined for 1-MQ (1a). On the basis of this result, 1-MNA analogues with dimethyl groups at C4- and C6-positions (5b) and a sterically demanding C2-acyl-thiofuranyl group at the N1 position (5c) were tested. Compound 5b exhibited slightly decreased potency (IC₅₀ = 11.8 μM) relative to 5a (Table 5) and was similar to that of 1-MQ (1a). Again,

Table 7. Related Structural Analogues with Poor NNMT Inhibitory Activity

Structure	Compound name, IC ₅₀ (μM) ^a	Structure	Compound name, IC ₅₀ (μM) ^a	Structure	Compound name, IC ₅₀ (μM) ^a
	7a, 161.4 ± 272.9		7b, >300 ^b		7c, >1000
	7d, >1000		7e, >1000		7f, >1000
	7g, >1000		7h, >1000		7i, >1000

^aIC₅₀ values are represented at mean ± SD of duplicate or more measurements. ^bCompound precipitated in solution at concentration >300 μM. Exact IC₅₀ could not be determined.

consistent with the general observations that sterically hindered substituents at the N1 position significantly reduce the activity of analogues within the NNMT substrate-binding site, analogue 7c was observed to have very poor activity (IC₅₀ > 1000 μM).

Inhibitory Activities of Benzimidazoliums/Benzothiazoliums and Other Structural Analogues. Lastly, other structurally related chemotypes, i.e., compounds containing benzimidazolium and benzothiazolium scaffolds (6a–f; Table 6) and other heteroaryl templates (7a–i; Table 7) were tested for NNMT inhibition. Compound 6a, with apolar methyl group substituents at both the N1 and N3 positions of the benzimidazole scaffold exhibited an IC₅₀ value of 16.7 μM, which was ~2-fold lower relative to 1-MNA (5a), 1-MQ (1a), and N2-methyl isoquinolinium analogue (4a). Consistent with results observed for additive groups to the 1-MQ scaffold, an ethyl substitution at the N1 position (6b) was well tolerated and generated comparable activity (IC₅₀ = 22.8 μM) to the parent structure 6a. This is supported, in part, by overlapping intermolecular interactions that are predicted to occur between ligands containing distinct core scaffolds (1-MQ, N2-methyl isoquinolinium, pyridinium, and benzimidazolium/benzothiazolium) and NNMT substrate-binding site residues; however, molecular docking studies also revealed dissimilar interactions for the ligands with the different scaffolds within the NNMT substrate-binding site (refer to Molecular Docking discussion below). For example, the C3-amino benzimidazolium analogue 6c demonstrated a ~5-fold higher IC₅₀ value (IC₅₀ = 82.4 μM) relative to the parent structure 6a; this was in contrast to the 1-MQ and N2-methyl isoquinolinium scaffolds where an amino group at the C3-position improved ligand activity (1d and 4b). Other analogues composed of the benzimidazolium (6d) and benzothiazolium scaffolds (6e) were very poor inhibitors of NNMT (IC₅₀ > 1000 μM). As summarized in Table 7, only analogues (7a,b) containing phenanthridinium and acridinium

structures showed even modest ability to inhibit NNMT (IC₅₀ values, 100–300 μM); all other tested chemotypes (7c–i) showed very poor NNMT inhibition (IC₅₀ > 1000 μM). Importantly, analogues containing tetrahydroquinoline/quinolone scaffolds (e.g., 7d, 7f) that were uncharged exhibited very poor NNMT inhibition, suggesting that a positive charge at the N1 position may be a necessary chemical feature for small molecule inhibitors of NNMT.

Structure-Based Docking between NNMT and Small Molecule Inhibitors. The Vina computer docking program was able to reproduce the NCA molecular orientation observed in the X-ray structure of the NNMT–NCA–SAH ternary complex²⁴ with an all atom root-mean-square deviation of 0.74 Å, suggesting that these calculations would be suitable to investigate likely orientations and intermolecular interactions of small molecule inhibitors bound to NNMT. Binding orientations and docking scores between NNMT and each of the ~44 combined quinolinium, isoquinolinium, pyridinium, and benzimidazolium analogues containing N-methyl substituents, respectively, were calculated. As shown in Figure 2 for the combined set of analogues, a positive linear correlation ($r = 0.63$, $R^2 = 0.4$, $P[\text{two-tailed}] = 0.0003$) was observed between Vina docking score and log(IC₅₀) values. In these calculations, low (i.e., more negative) docking scores suggest more favorable binding conformations and intermolecular interactions between the ligand and macromolecular target. Consistent with this observation, analogues that were potent NNMT inhibitors (e.g., compounds 1k, 1t; IC₅₀ = 1.2–1.8 μM) had the lowest calculated Vina docking scores (scores between –8.3 and –8.1). Conversely, many analogues (e.g., per-methylated compounds 3e,f) that were either poor NNMT inhibitors (IC₅₀ > 1000 μM) or failed to inhibit NNMT had higher calculated Vina docking scores (scores between –6.0 and –5.0) or did not bind in the nicotinamide binding pocket. Taken

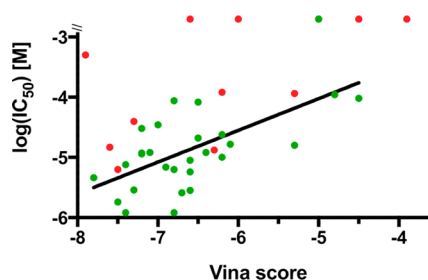


Figure 2. Correlation between the Vina docking scores and experimentally measured IC_{50} values for all analogues with methyl substitution at the N-position in each of the core scaffolds (41 compounds). Data points colored red correspond to analogues that docked outside the NNMT substrate-binding site. Pearson's correlation analysis performed on analogues that docked in the substrate-binding site (represented by green markers) indicated a positive linear correlation between calculated docking scores and $\log(IC_{50})$ ($r = 0.63$, $R^2 = 0.4$, $P[\text{two-tailed}] = 0.0003$).

together, Vina docking scores and inhibitor potencies were modestly correlative for many analogues containing the N1-methyl quinolinium scaffold (Figure 2), suggesting that docking calculations could serve as a predictive tool to guide the identification and design of small molecule NNMT inhibitors similar to other reported systems.³⁴ However, there were

exceptional N1-methylquinolinium ligands and analogues containing other chemical scaffolds (e.g., N2-methyl isoquinolinium, benzimidazolium) that were inconsistent, likely, in part, due to inherent limitations of the Vina computational program and/or inherent analogue properties. The Vina program makes assumptions on the protonation states/partial charge distribution in molecules not accounting for solvent, dipole, entropic, and tautomerization effects.³⁵ As a result, disparity between calculated docking scores and experimentally generated IC_{50} values were observed for some of the tested analogues. For example, analogues with relatively good docking scores (e.g., analogues **1s**, **2l**; docking scores between -7 and -8) exhibited poor IC_{50} values ($>500 \mu\text{M}$) and improvements imparted by C6-fluoro substitutions in the IC_{50} values compared to the nonfluorinated derivatives, presumably via enhanced dipolar interactions, were not truly reflected in the docking scores generated by the Vina calculations [e.g., analogues **1a** ($IC_{50} = 12.1 \mu\text{M}$) and **1m** ($IC_{50} = 5.7 \mu\text{M}$) had similar Vina docking scores ~ -7.7].

Vina docking calculations can predict likely orientations and conformations of small molecules bound to a target protein. 1-methylquinolinium (**1a**) was used to establish a prototypical structure for 1-MQ analogues bound to the NNMT substrate-binding pocket (Figure 3). The predicted binding orientation of 1-MQ (and related analogues) was similar to the bound

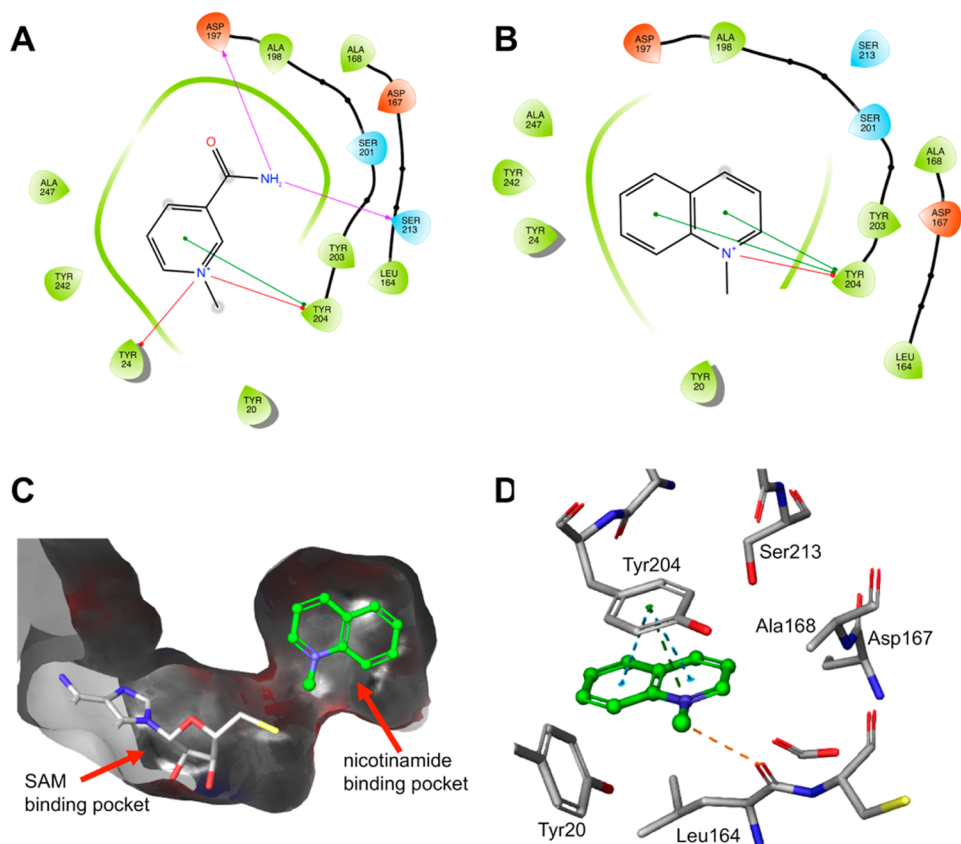


Figure 3. Bound orientation and intermolecular interactions between representative inhibitors and NNMT as calculated by the Vina molecular docking program. (A) 2-D schematic of the intermolecular interactions between NNMT and bound 1-methylnicotinamide (**1a**). (B) 2-D schematic of the intermolecular interactions between NNMT and bound 1-methylquinolinium (**1a**). (C) 3-D representation of the orientation of 1-methylquinolinium (**1a**) in the NNMT substrate-binding site and positioned relative to the SAM binding pocket. (D) 3-D representation of the intermolecular interactions between NNMT and bound 1-methylquinolinium (**1a**). Potential cation- π interactions are depicted by red arrows, π - π interactions are shown by green arrows, and hydrogen bonds are shown by purple arrows. Figures were produced with Maestro 11 (Schrodinger LLC, New York, NY).³⁷

structures of the endogenous substrate NCA and docked 1-MNA, with the N1 atoms of these ligands superimposable and with similar intermolecular interactions to residues within the NNMT substrate-binding pocket (Figure 3A,B). Moreover, the inhibitors were positioned in the nicotinamide binding pocket such that their N1-methyl groups were directed toward the adjacent SAM binding pocket (Figure 3C). 1-MQ and related analogues are predicted to form strong π - π , cation- π , and hydrophobic interactions with residues Tyr204 and Leu164 that define the apolar pocket surrounding the quinolinium N1-containing ring (Figure 3B,D), similar to the manner in which these aromatic residues interact with the pyridine ring of NCA in the NNMT substrate-binding site.²⁴ In addition, NNMT residues Ala198, Tyr242, and Tyr 24 were also indicated to contact via hydrophobic interactions with the quinolinium ring of 1-MQ (Figure 3B,D), two of which (Ala198 and Tyr242) have also been indicated to contact with the pyridinium ring of the substrate NCA and 1-MNA (Figure 3A). Further, the NCA amide group has been reported to form hydrogen bonds with the hydroxyl groups of Ser201/Ser213 residues and the Asp197 carboxylate.^{24,24} The predicted binding orientation of quinolinium analogue **1k**, however, suggests that the C5-amino group forms hydrogen bonds with Ser201 and hydrophobic interactions with Ser213 and Tyr20 (figure not shown). These distinct predicted interactions between analogue **1k** and NNMT compared to NCA suggest more favorable intermolecular bonding interactions with residues within the NNMT substrate-binding pocket, which is supported by a lower Vina docking score (Vina score = -8.1) for **1k** relative to 1-MNA (Vina score = -6.8) and the potent inhibitory activity exhibited by this analogue ($IC_{50} = 1.2 \mu M$).

The predicted conformations, binding orientations, and intermolecular interactions with NNMT residues for the most potent analogues with the pyridinium scaffold (1,2,4-trimethyl-5-carboxamidepyridinium, **5b**), benzimidazolium scaffold (1,2,3-trimethyl-1*H*-3,1-benzimidazol-3-ium, **6a**), and *N*2-methyl isoquinolinium scaffold (3-amine-2-methylisoquinolinim, **4b**) were examined and are summarized below. Inhibitors with different chemotypes were predicted to bind NNMT via hydrophobic interactions with the same aromatic residues (Leu164 and Tyr204) in the apolar substrate-binding pocket and make additional contacts with apolar atoms of Tyr24, Tyr242, and Ala198 around the respective scaffold ring structures relative to the prototype analogue **1k**. Analogues **5b** and **6a** with the pyridinium and benzimidazolium scaffolds, respectively, either formed only hydrogen bonds or hydrophobic contacts with Ser201/213 residues and made additional hydrophobic contacts with NNMT residues (e.g., **5b**, Asp167, Ala247; **6a**, Ala168, Asp167, Asp197) compared to **1k**, which potentially rendered these inhibitors less potent (at least ~10-fold lower potency relative to **1k**). Lastly, the predicted orientation of isoquinolinium analogues (e.g., **4b**) was shifted within the NNMT substrate-binding pocket relative to the quinolinium analogues. Specifically, the carbon atoms around the *N*2-methyl isoquinolinium rings were predicted to form distinct hydrophobic interactions with NNMT residues Tyr203 and Ala247 and more importantly form hydrogen bond and hydrophobic interactions with the phenol hydroxyl group and ring carbon atoms in the backbone of Tyr20 residue, respectively. Given that Tyr20 is critical for the functional activity of NNMT²⁴ and the alignment of both methyl donor and acceptor molecules (SAM and NCA) in the binding

pocket,²⁴ interactions with this residue might be relevant in guiding the inhibitor activity.

Summary of SAR for 1-MQ Analogues. The most potent NNMT inhibitor analogues identified in the current study (e.g., **1k**, **2j**; $IC_{50} \sim 1.2 \mu M$) contained the quinolinium scaffold. These compounds were predicted to bind the NNMT substrate-binding pocket analogous to NCA and exhibited favorable intermolecular interactions with NNMT residues. A predictive SAR developed for this series of analogues highlights a few important chemical features required for potent NNMT inhibition as summarized in Figure 4: (i) apolar methyl

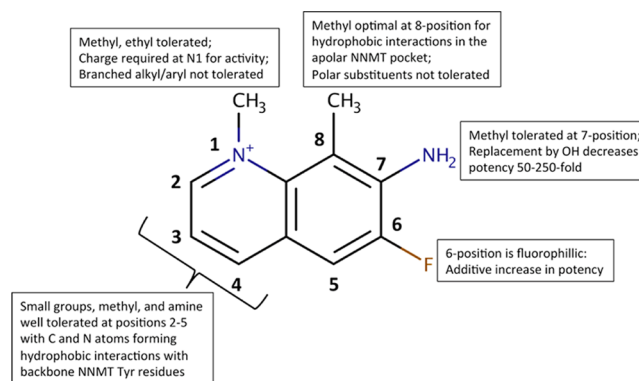


Figure 4. SAR summary for analogues containing the quinolinium scaffold (information abstracted from Tables 1–3).

substitutions at N1 and C8 positions promote strong hydrophobic interactions with aromatic NNMT residues (Leu164, Tyr204), and the positive charge on the N1 atom is required to retain potent inhibitory activity; (ii) methyl or amino substituents at C2–C5-, and C7-positions provide favorable C and N atoms that can contact with Tyr (Tyr20, Tyr24, Tyr242) and Ser (Ser201 and Ser213) residues via multiple hydrophobic and/or hydrogen bond interactions; and (iii) an electron-withdrawing fluoro substitution at the C6-position engages in multipolar interactions and significantly enhances analogue potency.

CONCLUSIONS

Exploration of an initial series of commercially available and synthesized *N*-methylated analogues of different chemotypes, including quinolinium, isoquinolinium, pyrididum, and benzimidazolium/benzothiazolium, resulted in the rapid development of structure–activity relationships (SARs) for NNMT inhibitors demonstrating >1000-fold range of activity. Computer-based docking of inhibitors to the NNMT NCA substrate-binding site produced a robust correlation between ligand–enzyme interaction docking scores and experimentally established IC_{50} values. Computational calculations and predicted binding orientation of inhibitors enabled identification of NNMT residues responsible for protein–ligand intermolecular interactions. The quinolinium analogue series that demonstrated significant NNMT inhibition were further expanded by synthesis, guided in part by calculations to identify analogues with improved docking scores and binding. Potent quinolinium analogues identified in the current study exhibited very low micromolar potency ($IC_{50} \sim 1 \mu M$) that fully correlated with very low ligand–enzyme docking scores. The SAR described herein demonstrates quinolinium as a promising scaffold to selectively bind to the NNMT substrate-binding site

with a confirmation analogous to the endogenous NNMT substrate NCA and highlights some of the key structural features of quinolinium analogues for NNMT inhibition. These SAR results motivate future exploration of the chemical space surrounding the template moieties to develop potent, selective, and drug-like NNMT inhibitors. Ongoing research will investigate selectivity, confirm inhibitor activities using orthogonal assays, and develop potent NNMT inhibitors with improved “drug-like” physicochemical properties. Future studies will elucidate inhibitor mechanism-of-action and the structures of the NNMT–SAM–inhibitor ternary complexes, which will validate the molecular predictions derived from the current findings.

EXPERIMENTAL SECTION

Chemistry. Analogues and Chemicals. PubChem and Zinc similarity search programs were employed to identify commercially available analogues containing quinolinium, isoquinolinium, pyridinium, benzimidazolium, and benzothiazolium core structures and the analogues were purchased from established commercial suppliers, including Sigma-Aldrich (St. Louis, MO), Chembridge Corporation (San Diego, CA), ChemDiv (San Diego, CA), Specs (Hopkinton, RI), Cayman (Ann Arbor, MI), and Pfaltz & Bauer (Waterbury, CT). The identity of all the tested compounds was confirmed by ^1H NMR and HPLC-MS, and the purity was ensured to be $\geq 95\%$ (see Supporting Information for representative examples of HPLC analyses for compound purity). SAM was obtained from Sigma-Aldrich and nicotinamide from Fluka Analytical (Kwazulu Natal, South Africa; distributed by Sigma-Aldrich in the USA). 1-MNA chloride and S-5'-adenosylhomocysteine (SAH) were obtained from Cayman Chemical Company (Ann Arbor, MI). All compounds were made in double-distilled water.

General Procedures. Unless otherwise indicated, all reactions were conducted in standard commercially available glassware using standard synthetic chemistry methods and setup. All air- and moisture-sensitive reactions were performed under nitrogen atmosphere with dried solvents and glassware under anhydrous conditions. Starting materials and reagents were commercial compounds of the highest purity available and were used without purification. Solvents used for reactions were indicated as of commercial dry or extra-dry or analytical grade. Analytical thin layer chromatography was performed on aluminum plates coated with Merck Kieselgel 60F254 and visualized by UV irradiation (254 nm) or by staining with a solution of potassium permanganate. Flash column chromatography was performed on Biotage Isolera One 2.2 using commercial columns that were prepacked with Merck Kieselgel 60 (230–400 mesh) silica gel. Final compounds for biological testing are all $\geq 95\%$ purity as determined by HPLC-MS and ^1H NMR.

NMR. ^1H NMR experiments were recorded on Agilent DD2 400 MHz spectrometers at ambient temperature. Samples were dissolved and prepared in deuterated solvents (CDCl_3 , CD_3OD , and $\text{DMSO}-d_6$) with residual solvents being used as the internal standard in all cases. All deuterated solvent peaks were corrected to the standard chemical shifts (CDCl_3 , $d_{\text{H}} = 7.26$ ppm; CD_3OD , $d_{\text{H}} = 3.31$ ppm; $\text{DMSO}-d_6$, $d_{\text{H}} = 2.50$ ppm). Spectra were all manually integrated after automatic baseline correction. Chemical shifts (δ) are given in parts per million (ppm), and coupling constants (J) are given in Hertz (Hz). The proton spectra are reported as follows: d (multiplicity, coupling constant J , number of protons). The following abbreviations were used to explain the multiplicities: app = apparent, b = broad, d = doublet, dd = doublet of doublets, ddd = doublet of doublet of doublets, dddd = doublet of doublet of doublet of doublets, m = multiplet, s = singlet, t = triplet.

HPLC-MS. All samples were analyzed on Agilent 1290 series HPLC system comprised of binary pumps, degasser, UV detector, and autosampler coupled to an Agilent 6150 mass spectrometer. Purity was determined via UV detection with a bandwidth of 170 nm in the range from 230 to 400 nm. The general LC parameters were as follows:

Column, Zorbax Eclipse Plus C18, size 2.1 mm \times 50 mm; solvent A, 0.10% formic acid in water; solvent B, 0.00% formic acid in acetonitrile; flow rate, -0.7 mL/min; gradient, 5% B to 95% B in 5 min and hold at 95% B for 2 min; UV detector, channel 1 = 254 nm, channel 2 = 254 nm. Mass detector Agilent Jet Stream–Electron Ionization (AJS-ES).

General Procedure A: Quinolinyl or Isoquinolinyl Ring N-Alkylation Using MeI. A mixture of appropriate quinoline or isoquinoline derivative (1 equiv) and MeI (1.5 equiv unless otherwise indicated) in IPA (0.5M) was heated at 90 °C for 12 h. The reaction was cooled to ambient temperature, and the resulting precipitate was isolated by vacuum filtration, washed with a mixture of IPA/Et₂O (v:v/1:1), and dried in vacuo.

General Procedure B: Quinolinyl or Isoquinolinyl Ring N-Alkylation Using MeOTf. A mixture of appropriate quinoline or isoquinoline derivative (1 equiv) and MeOTf (3 equiv unless otherwise indicated) in toluene (0.2M) was heated at 100 °C for 12 h. The reaction was cooled to ambient temperature and Et₂O added to induce precipitation. The resulting precipitate was isolated by vacuum filtration, washed with Et₂O, and dried in vacuo.

1,2-Dimethylquinolin-1-ium Trifluoromethanesulfonate (1b). According to general procedure B, the title compound was obtained as pale-orange powder (89% yield). ^1H NMR (400 MHz, $\text{DMSO}-d_6$) δ 9.08 (d, $J = 8.4$ Hz, 1H), 8.58 (d, $J = 9.2$ Hz, 1H), 8.39 (d, $J = 8.0$ Hz, 1H), 8.22 (dd, $J = 8.4, 7.6$ Hz, 1H), 8.10 (d, $J = 8.8$ Hz, 1H), 7.99 (dd, $J = 8.4, 7.6$ Hz, 1H), 4.44 (s, 3H), 3.07 (s, 3H). HPLC-MS (AJS-ES): R_t 1.13 min, m/z 158.2 [$\text{M}-\text{OSO}_2\text{CF}_3$].

2-Amino-1-methylquinolin-1-ium iodide (1c). According to general procedure A, the title compound was obtained as gray powder (26% yield). ^1H NMR (400 MHz, $\text{DMSO}-d_6$) δ 9.45 (br, 1H), 8.87 (br, 1H), 8.34 (d, $J = 9.2$ Hz, 1H), 8.01 (d, $J = 8.8$ Hz, 1H), 7.98 (d, $J = 8.8$ Hz, 1H), 7.87 (dd, $J = 8.4, 7.6$ Hz, 1H), 7.57 (dd, $J = 7.6, 7.6$ Hz, 1H), 7.17 (d, $J = 9.2$ Hz, 1H), 3.87 (s, 3H). HPLC-MS (AJS-ES): R_t 1.31 min, m/z 159.1 [$\text{M}-\text{I}$].

3-Amino-1-methylquinolin-1-ium iodide (1d). According to general procedure A, the title compound was obtained as orange powder (33% yield). ^1H NMR (400 MHz, $\text{DMSO}-d_6$) δ 8.81 (s, 1H), 8.21 (d, $J = 8.8$ Hz, 1H), 8.07 (d, $J = 7.2$ Hz, 1H), 7.98 (s, 1H), 7.78 (m, 2H), 6.56 (br, 2H), 4.51 (s, 3H). HPLC-MS (AJS-ES): R_t 1.08 min, m/z 159.1 [$\text{M}-\text{I}$].

1,3-Dimethylquinolin-1-ium trifluoromethanesulfonate (1e). According to general procedure A, the title compound was obtained as white powder (93% yield). ^1H NMR (400 MHz, $\text{DMSO}-d_6$) δ 9.47 (s, 1H), 9.08 (s, 1H), 8.46 (d, $J = 9.2$ Hz, 1H), 8.35 (d, $J = 9.2$ Hz, 1H), 8.21 (ddd, $J = 7.6, 6.8, 1.6$ Hz, 1H), 8.02 (ddd, $J = 7.6, 7.6, 0.8$ Hz, 1H), 4.60 (s, 3H), 2.64 (s, 3H). HPLC-MS (AJS-ES): R_t 0.39 min, m/z 158.1 [$\text{M}-\text{OSO}_2\text{CF}_3$].

1-Methyl-3-(methylamino)quinolin-1-ium iodide (1f). According to general procedure A, the title compound was obtained as orange powder (72% yield). ^1H NMR (400 MHz, $\text{DMSO}-d_6$) δ 8.90 (d, $J = 2.4$ Hz, 1H), 8.22 (dd, $J = 4.8, 4.4$ Hz, 1H), 8.10 (dd, $J = 4.8, 4.4$ Hz, 1H), 7.97 (d, $J = 1.6$ Hz, 1H), 7.78 (dd, $J = 4.8, 4.4$ Hz, 1H), 7.13 (br, 1H), 4.54 (s, 3H), 2.90 (s, 3H). HPLC-MS (AJS-ES): R_t 0.78 min, m/z 173.1 [$\text{M}-\text{I}$].

1-Methyl-3-(phenylamino)quinolin-1-ium iodide (1h). According to general procedure A, the title compound was obtained as orange–yellow powder (59% yield). ^1H NMR (400 MHz, $\text{DMSO}-d_6$) δ 9.33 (s, 1H), 9.17 (d, $J = 2.4$ Hz, 1H), 8.57 (d, $J = 2.0$ Hz, 1H), 8.31 (d, $J = 8.8$ Hz, 1H), 8.23 (d, $J = 8.0$ Hz, 1H), 7.93 (dd, $J = 8.0, 7.6$ Hz, 1H), 7.85 (dd, $J = 8.0, 6.8$ Hz, 1H), 7.44 (d, $J = 8.0$ Hz, 1H), 7.41 (d, $J = 7.6$ Hz, 1H), 7.34 (s, 1H), 7.32 (s, 1H), 7.11 (dd, $J = 8.0, 7.2$ Hz, 1H), 4.59 (s, 3H). HPLC-MS (AJS-ES): R_t 1.48 min, m/z 235.2 [$\text{M}-\text{I}$].

4-Amino-1-methylquinolin-1-ium iodide (1j). According to general procedure A, the title compound was obtained as gray powder (78% yield). ^1H NMR (400 MHz, $\text{DMSO}-d_6$) δ 8.97 (s, 2H), 8.51 (d, $J = 7.6$ Hz, 1H), 8.48 (d, $J = 8.4$ Hz, 1H), 8.06 (d, $J = 3.6$ Hz, 2H), 7.77 (m, 1H), 6.78 (d, $J = 7.2$ Hz, 1H), 4.11 (s, 3H). HPLC-MS (AJS-ES): R_t 0.69 min, m/z 159.1 [$\text{M}-\text{I}$].

5-Amino-1-methylquinolin-1-ium iodide (1k). According to general procedure A, the title compound was obtained using

stoichiometric amount of MeI (1 equiv) to isolate the product as red powder (62% yield). $^1\text{H NMR}$ (400 MHz, $\text{DMSO-}d_6$) δ 9.32 (d, $J = 8.4$ Hz, 1H), 9.28 (d, $J = 5.6$ Hz, 1H), 7.89 (dd, $J = 8.4, 8.0$ Hz, 1H), 7.85 (d, $J = 5.6$ Hz, 1H), 7.35 (d, $J = 8.8$ Hz, 1H), 7.11 (br, 2H), 7.02 (d, $J = 8.0$ Hz, 1H), 4.42 (s, 3H). HPLC-MS (AJS-ES): R_t 0.39 min, m/z 159.1 [M-I].

1,5-Dimethylquinolin-1-ium trifluoromethanesulfonate (1l). According to general procedure B, the title compound was obtained as white powder (99% yield). $^1\text{H NMR}$ (400 MHz, $\text{DMSO-}d_6$) δ 9.48 (d, $J = 5.6$ Hz, 1H), 9.35 (d, $J = 8.8$ Hz, 1H), 8.35 (d, $J = 8.8$ Hz, 1H), 8.17 (dd, $J = 8.4, 1.6$ Hz, 1H), 8.16 (d, $J = 8.8$ Hz, 1H), 7.90 (d, $J = 7.2$ Hz, 1H), 4.63 (s, 3H), 2.86 (s, 3H). HPLC-MS (AJS-ES): R_t 0.41 min, m/z 158.1 [M-OSO₂CF₃].

6-Fluoro-1-methylquinolin-1-ium iodide (1m). According to general procedure A, the title compound was obtained as yellow powder (75% yield). $^1\text{H NMR}$ (400 MHz, $\text{DMSO-}d_6$) δ 9.52 (s, 1H), 9.23 (d, $J = 8.8$ Hz, 1H), 8.64 (dd, $J = 9.6, 4.4$ Hz, 1H), 8.37 (dd, $J = 8.8, 2.8$ Hz, 1H), 8.26 (dddd, $J = 9.2, 9.2, 2.8, 2.0$ Hz, 1H), 8.21 (dd, $J = 8.4, 5.6$ Hz, 1H), 4.66 (s, 3H). HPLC-MS (AJS-ES): R_t 0.37 min, m/z 162.1 [M-I].

6-Amino-1-methylquinolin-1-ium iodide (1o). According to general procedure A, the title compound was obtained as orange-brown powder (58% yield). $^1\text{H NMR}$ (400 MHz, $\text{DMSO-}d_6$) δ 8.94 (s, 1H), 8.77 (d, $J = 9.2$ Hz, 1H), 8.18 (d, $J = 9.2$ Hz, 1H), 7.83 (m, 1H), 7.58 (d, $J = 9.2$ Hz, 1H), 7.11 (s, 1H), 6.46 (br, 2H), 4.48 (s, 3H). HPLC-MS (AJS-ES): R_t 0.74 min, m/z 159.1 [M-I].

7-Amino-1-methylquinolin-1-ium iodide (1q). According to general procedure A, the title compound was obtained using stoichiometric amount of MeI (1 equiv) to isolate the product as orange-brown powder (56% yield). $^1\text{H NMR}$ (400 MHz, $\text{DMSO-}d_6$) δ 8.92 (d, $J = 5.6$ Hz, 1H), 8.71 (d, $J = 8.0$ Hz, 1H), 8.02 (d, $J = 9.2$ Hz, 1H), 7.46 (dd, $J = 7.6, 6.4$ Hz, 1H), 7.38 (br, 2H), 7.29 (dd, $J = 9.2, 1.6$ Hz, 1H), 6.93 (d, $J = 1.2$ Hz, 1H), 4.23 (s, 3H). HPLC-MS (AJS-ES): R_t 0.52 min, m/z 159.1 [M-I].

1,7-Dimethylquinolin-1-ium Trifluoromethanesulfonate (1r). According to general procedure B, the title compound was obtained as white powder (87% yield). $^1\text{H NMR}$ (400 MHz, $\text{DMSO-}d_6$) δ 9.41 (d, $J = 6.0$ Hz, 1H), 9.20 (d, $J = 8.4$ Hz, 1H), 8.36 (d, $J = 8.4$ Hz, 1H), 8.34 (s, 1H), 8.08 (dd, $J = 8.4, 6.0$ Hz, 1H), 7.91 (d, $J = 8.4$ Hz, 1H), 4.59 (s, 3H), 2.72 (s, 3H). HPLC-MS (AJS-ES): R_t 0.41 min, m/z 158.1 [M-OSO₂CF₃].

3-Amino-6-fluoro-1-methylquinolin-1-ium iodide (2j). According to general procedure A, the title compound was obtained as yellow powder (58% yield). $^1\text{H NMR}$ (400 MHz, $\text{DMSO-}d_6$) δ 8.84 (d, $J = 2.0$ Hz, 1H), 8.35 (dd, $J = 9.6, 4.4$ Hz, 1H), 7.99 (dd, $J = 9.2, 2.8$ Hz, 1H), 7.94 (d, $J = 2.0$ Hz, 1H), 7.76 (ddd, $J = 8.8, 8.8, 3.2$ Hz, 1H), 6.78 (br, 2H), 4.56 (s, 3H). HPLC-MS (AJS-ES): R_t 0.22 min, m/z 177.1 [M-I].

1,8-Dimethyl-5-(trifluoromethyl)quinolin-1-ium Trifluoromethanesulfonate (2k). According to general procedure B, the title compound was obtained using excess amount of MeOTf (5 equiv) to isolate the product as pale-gray powder (69% yield). $^1\text{H NMR}$ (400 MHz, $\text{DMSO-}d_6$) δ 9.56 (d, $J = 6.0$ Hz, 1H), 9.24 (d, $J = 8.8$ Hz, 1H), 8.38 (d, $J = 7.6$ Hz, 1H), 8.29 (dd, $J = 8.8, 5.6$ Hz, 1H), 8.21 (d, $J = 7.6$ Hz, 1H), 4.89 (s, 3H), 3.15 (s, 3H). HPLC-MS (AJS-ES): R_t 0.92 min, m/z 226.1 [M-OSO₂CF₃].

4-Chloro-1-methyl-8-(trifluoromethyl)quinolin-1-ium Trifluoromethanesulfonate (2l). According to general procedure B, the title compound was obtained using excess amount of MeOTf (5 equiv) to isolate the product as pale gray powder (88% yield). $^1\text{H NMR}$ (400 MHz, $\text{DMSO-}d_6$) δ 8.56 (m, 1H), 8.33–8.10 (m, 2H), 7.59 (m, 1H), 6.47 (m, 1H), 3.93 (m, 3H). HPLC-MS (AJS-ES): R_t 3.01 min, m/z 246.1 [M-OSO₂CF₃].

2,3-Diamino-1-methylquinolin-1-ium iodide (2m). According to general procedure A, the title compound was obtained as tan powder (30% yield). $^1\text{H NMR}$ (400 MHz, $\text{DMSO-}d_6$) δ 8.76 (br, 2H), 7.89 (d, $J = 8.4$ Hz, 1H), 7.72 (d, $J = 8.0$ Hz, 1H), 7.54 (dd, $J = 8.0, 7.2$ Hz, 1H), 7.43 (dd, $J = 7.6, 7.6$ Hz, 1H), 7.35 (br, 1H), 5.94 (br, 2H), 3.95 (s, 3H). HPLC-MS (AJS-ES): R_t 1.41 min, m/z 174.1 [M-I].

1,2,8-Trimethylquinolin-1-ium Trifluoromethanesulfonate (2n).

According to general procedure B, the title compound was obtained as pale-tan powder (84% yield). $^1\text{H NMR}$ (400 MHz, $\text{DMSO-}d_6$) δ 9.01 (d, $J = 8.4$ Hz, 1H), 8.18 (d, $J = 8.0$ Hz, 1H), 8.04 (d, $J = 8.4$ Hz, 1H), 8.02 (d, $J = 8.4$ Hz, 1H), 7.83 (dd, $J = 7.6, 7.6$ Hz, 1H), 4.45 (s, 3H), 3.03 (s, 3H), 2.97 (s, 3H). HPLC-MS (AJS-ES): R_t 0.31 min, m/z 172.1 [M-OSO₂CF₃].

1,2,6-Trimethylquinolin-1-ium iodide (2o). According to general procedure A, the title compound was obtained as yellow-orange powder (36% yield). $^1\text{H NMR}$ (400 MHz, $\text{DMSO-}d_6$) δ 8.98 (d, $J = 8.4$ Hz, 1H), 8.49 (d, $J = 9.2$ Hz, 1H), 8.16 (s, 1H), 8.08 (m, 1H), 8.06 (m, 1H), 4.42 (s, 3H), 3.05 (d, $J = 4.0$ Hz, 3H), 2.60 (s, 3H). HPLC-MS (AJS-ES): R_t 1.00 min, m/z 172.1 [M-I].

1,2,4,8-Tetramethylquinolin-1-ium Trifluoromethanesulfonate (3c). According to general procedure B, the title compound was obtained as white powder (94% yield). $^1\text{H NMR}$ (400 MHz, $\text{DMSO-}d_6$) δ 8.25 (d, $J = 8.4$ Hz, 1H), 8.00 (d, $J = 6.8$ Hz, 1H), 7.96 (s, 1H), 7.84 (dd, $J = 8.0, 7.6$ Hz, 1H), 4.36 (s, 3H), 2.96 (s, 3H), 2.93 (s, 3H), 2.88 (s, 3H). HPLC-MS (AJS-ES): R_t 0.85 min, m/z 186.2 [M-OSO₂CF₃].

1,2,4,5,8-Pentamethylquinolin-1-ium Trifluoromethanesulfonate (3d). According to general procedure B, the title compound was obtained as tan powder (93% yield). $^1\text{H NMR}$ (400 MHz, $\text{DMSO-}d_6$) δ 7.83 (s, 1H), 7.80 (d, $J = 7.6$ Hz, 1H), 7.61 (d, $J = 8.0$ Hz, 1H), 4.24 (s, 3H), 3.04 (s, 3H), 2.91 (s, 6H), 2.78 (s, 3H). HPLC-MS (AJS-ES): R_t 1.01 min, m/z 200.2 [M-OSO₂CF₃].

1,2,4,7,8-Pentamethylquinolin-1-ium Trifluoromethanesulfonate (3e). According to general procedure B, the title compound was obtained as white powder (70% yield). $^1\text{H NMR}$ (400 MHz, $\text{DMSO-}d_6$) δ 8.03 (s, 1H), 7.91 (s, 1H), 7.85 (s, 1H), 4.35 (s, 3H), 2.93 (s, 3H), 2.90 (s, 3H), 2.85 (s, 3H), 2.55 (s, 3H). HPLC-MS (AJS-ES): R_t 1.11 min, m/z 200.2 [M-OSO₂CF₃].

1,2,4,7,8-Pentamethylquinolin-1-ium Trifluoromethanesulfonate (3f). According to general procedure B, the title compound was obtained as white powder (87% yield). $^1\text{H NMR}$ (400 MHz, $\text{DMSO-}d_6$) δ 8.13 (d, $J = 8.4$ Hz, 1H), 7.87 (s, 1H), 7.79 (d, $J = 8.4$ Hz, 1H), 4.28 (s, 3H), 2.94 (s, 3H), 2.86 (s, 3H), 2.67 (s, 3H), 2.57 (s, 3H). HPLC-MS (AJS-ES): R_t 1.04 min, m/z 200.2 [M-OSO₂CF₃].

5-Fluoro-1,2,4,8-tetramethylquinolin-1-ium Trifluoromethanesulfonate (3g). According to general procedure B, the title compound was obtained as tan powder (89% yield). $^1\text{H NMR}$ (400 MHz, $\text{DMSO-}d_6$) δ 7.99 (dd, $J = 7.6, 6.8$ Hz, 1H), 7.95 (s, 1H), 7.70 (dd, $J = 11.2, 8.8$ Hz, 1H), 4.32 (s, 3H), 2.95 (s, 6H), 2.86 (s, 3H). HPLC-MS (AJS-ES): R_t 0.87 min, m/z 204.2 [M-OSO₂CF₃].

7-Fluoro-1,2,4,8-tetramethylquinolin-1-ium Trifluoromethanesulfonate (3h). According to general procedure B, the title compound was obtained as white powder (78% yield). $^1\text{H NMR}$ (400 MHz, $\text{DMSO-}d_6$) δ 8.37 (dd, $J = 9.6, 6.8$ Hz, 1H), 7.95 (s, 1H), 7.89 (dd, $J = 9.2, 9.2$ Hz, 1H), 4.35 (s, 3H), 2.96 (s, 3H), 2.89 (s, 3H), 2.74 (s, 3H). HPLC-MS (AJS-ES): R_t 0.86 min, m/z 204.2 [M-OSO₂CF₃].

3-Amino-2-methylisoquinolin-2-ium iodide (4b). According to general procedure A, the title compound was obtained as tan-orange powder (40% yield). $^1\text{H NMR}$ (400 MHz, $\text{DMSO-}d_6$) δ 9.36 (s, 1H), 7.93 (d, $J = 8.4$ Hz, 1H), 7.81 (d, $J = 8.8$ Hz, 1H), 7.75 (dd, $J = 6.4, 0.8$ Hz, 1H), 7.71 (br, 2H), 7.41 (ddd, $J = 7.6, 7.6, 0.8$ Hz, 1H), 7.34 (s, 1H), 4.03 (s, 3H). HPLC-MS (AJS-ES): R_t 1.25 min, m/z 159.1 [M-I].

4-Bromo-2-methylisoquinolin-2-ium iodide (4c). According to general procedure A, the title compound was obtained using excess MeI (5 equiv) to isolate the product as tan-yellow powder (99% yield). $^1\text{H NMR}$ (400 MHz, $\text{DMSO-}d_6$) δ 10.09 (m, 1H), 9.24 (s, 1H), 8.56 (d, $J = 8.0$ Hz, 1H), 8.43–8.33 (m, 2H), 8.17 (dd, $J = 8.0, 8.0$ Hz, 1H), 4.45 (d, $J = 4.0$ Hz, 3H). HPLC-MS (AJS-ES): R_t 0.63 min, m/z 222.0, 224.0 [M-I].

6-Amino-2-methylisoquinolin-2-ium iodide (4d). According to general procedure A, the title compound was obtained as tan powder (68% yield). $^1\text{H NMR}$ (400 MHz, $\text{DMSO-}d_6$) δ 9.21 (s, 1H), 8.14 (dd, $J = 6.8, 1.2$ Hz, 1H), 8.00 (d, $J = 8.8$ Hz, 1H), 7.81 (d, $J = 6.8$ Hz, 1H), 7.35 (br, 2H), 7.27 (dd, $J = 8.8, 2.0$ Hz, 1H), 6.89 (d, $J = 1.6$ Hz, 1H), 4.16 (s, 3H). HPLC-MS (AJS-ES): R_t 0.78 min, m/z 159.1 [M-I].

6-Bromo-2-methylisoquinolin-2-ium Iodide (4e). According to general procedure A, the title compound was obtained using excess MeI (5 equiv) to isolate the product as brown–gray powder (99% yield). ¹H NMR (400 MHz, DMSO-*d*₆) δ 10.04 (s, 1H), 8.74 (d, *J* = 6.4 Hz, 1H), 8.69 (s, 1H), 8.49 (d, *J* = 6.4 Hz, 1H), 8.41 (d, *J* = 8.8 Hz, 1H), 8.21 (m, 1H), 4.45 (s, 3H). HPLC-MS (AJS-ES): *R*_f 1.25 min, *m/z* 222.0, 224.0 [M-1].

7-Amino-2-methylisoquinolin-2-ium Iodide (4f). According to general procedure A, the title compound was obtained as orange–yellow powder (53% yield). ¹H NMR (400 MHz, DMSO-*d*₆) δ 9.48 (s, 1H), 8.23 (d, *J* = 6.8 Hz, 1H), 8.20 (d, *J* = 6.8 Hz, 1H), 7.99 (d, *J* = 8.8 Hz, 1H), 7.55 (dd, *J* = 8.8, 2.4 Hz, 1H), 7.13 (d, *J* = 2.0 Hz, 1H), 6.52 (br, 2H), 4.34 (s, 3H). HPLC-MS (AJS-ES): *R*_f 0.78 min, *m/z* 159.1 [M-1].

Biology. Expression and Purification of Recombinant hNNMT. Because previous studies had demonstrated that a triple mutant human NNMT (tm-hNNMT; containing three site-directed mutations at surface exposed residues well removed from the catalytic sites) and wild-type NNMT had similar activities and kinetic parameters,²⁴ the tm-hNNMT enzyme was utilized in these current studies to facilitate planned crystallographic analysis of inhibitor:NNMT complexes and to enable direct comparison to previous kinetic studies. The tm-hNNMT sequence was cloned into an isopropyl-β-D-1-thiogalactopyranoside (IPTG)-inducible plasmid pJ401 expression vector was purchased from DNA 2.0 (Menlo Park, CA). tm-hNNMT was expressed in competent *Escherichia coli* BL21/DE3 cells and purified using a nickel-based ion affinity chromatography procedure as described in detail previously.³³

NNMT Activity Assay: HPLC Instrumentation and Chromatographic Conditions. An HPLC-UV method for the detection of NNMT catalyzed product 1-MNA was developed by modifying a previously reported protocol.²⁶ A Shimadzu 10AVP HPLC System (Shimadzu, Kyoto, Japan) with manual sample injector was used to run the HPLC-UV method with mobile phase comprising of 10 mM 1-heptanesulfonate, 20 mM potassium phosphate monobasic [pH 3.1], 4% methanol, and 3% acetonitrile. Chromatographic separation was achieved on a Platinum EPS C18 100 Å 3 μm (length, 53 mm; internal diameter, 7 mm; maximum pressure, 5000 PSIG) analytical column (Alltech Associates, Inc., Deerfield, IL) at ambient temperature with a flow rate of the mobile phase maintained at 1 mL/min. Sample injection volume was 100 μL with a run time of 20 min per sample.

1-MNA Calibration Curve and NNMT Activity Assay. To establish a linear curve for the detection of 1-MNA peak, 10–0.3125 μM/100 μL half-fold serially diluted samples of 1-MNA were prepared in reaction buffer containing 1 mM Tris [pH 8.6], 1 mM DTT, 10% TCA, 4% methanol, and water. Similarly, samples of substrate NCA (100 μM), methyl donor SAM (5 μM), and SAH (5 μM) were run individually in reaction buffer (1 mM Tris [pH 8.6], 1 mM DTT, 10% TCA, 4% methanol, and water) to identify elution times and define substrate, cofactor, and product peaks. 1-MNA, NCA, SAM, and SAH peaks were detected using a wavelength of 265 nm. To determine NNMT activity, 5 μL of 10 mM NCA (in water) and 2.5 μL of 1 mM SAM (in water) were added/500 μL of reaction buffer. The reaction was initiated by adding 4 μL of 25 μM stock purified NNMT protein (final concentration of NNMT in the reaction was 200 nM) and incubated on a heat block at 37 °C for 6 min, following which the reaction was terminated by the addition of a mixture of 10% TCA and 4% methanol, vortexing for 5 s, and centrifuging at 14000g for 2 min to precipitate the protein. Peak area and peak height for 1-MNA were determined by running 100 μL of the supernatant using the chromatographic conditions described above. Reactions were run in the absence of NNMT as control samples in each experiment.

NNMT IC₅₀ Curves for Inhibitors. NNMT reaction products were analyzed by HPLC as described above and used to construct inhibition curves for 1-MQ, 1-MQ analogues, 2-methylisoquinolinium, 2-methylisoquinolinium analogues, and analogues containing pyridinium, benzimidazolium, and benzothiazolium cores. Compounds were initially tested for NNMT inhibition activity at 100 μM or 1 mM concentration (compounds with no activity at 100 μM were tested at 1 mM concentration). Compounds with >50% inhibitory activity at 1

mM were advanced to comprehensive concentration–response analysis (concentration range of 10 nM–1 mM/100 μL reaction). Otherwise, IC₅₀ values are reported as either >1000 μM or no observable inhibition (NI). Data were normalized and reported as % NNMT activity against concentrations tested (μM). IC₅₀ values were determined by three parameter nonlinear regression [inhibitor conc vs normalized % NNMT activity] fitted by least-squares method (Graphpad Prism 7.0, GraphPad Software Inc., La Jolla, CA). For compounds with IC₅₀ values lower than 20 μM and/or *R*² values for the curve fit <0.8, data sets were run in duplicates or triplicates and averaged for analyses.

Molecular Docking. Quinolinium, isoquinolinium, pyridinium, benzimidazolium, and benzothiazolium analogues were docked to substrate-binding site of NNMT [PDB 3ROD, monomer chain A]²⁴ using the AutoDock Vina program.³⁵ AutoDockTools (ADT) was used to add polar hydrogen atoms to the NNMT structure and parametrize the resultant structure using Autodock4 default atom types. Three-dimensional conformations for each small molecule structure was produced in MarvinSketch, converted to Mol2 format, and parametrized with ADT to establish rotatable bonds and atom types. The Vina program was used to calculate the lowest scoring pose/conformation for each analogue bound to NNMT, using a search box (24 × 24 × 24) centered within the nicotinamide binding pocket (search space centered at -29, -20, 4 Å) and an “exhaustiveness” parameter of 20. During docking calculations, the protein structure was fixed as determined from the crystal structure while docked ligands had conformational flexibility around identified rotatable bonds. Analogue conformations with the lowest (i.e., most negative) Vina docking scores corresponded to the bound inhibitor conformation with most favorable interactions within the substrate-binding site of the NNMT protein. A linear analysis using Pearson’s correlation was performed between calculated Vina docking scores and the logarithm of experimentally determined IC₅₀ [log(IC₅₀)] for the respective compounds (Graphpad Prism 7.0, GraphPad Software Inc., La Jolla, CA).

The predicted orientations and conformations generated from the Vina docking for analogues with the lowest IC₅₀ values within each scaffold series were analyzed using the AutoDock Tools (ADT) molecular graphics program. The structure of ligands docked to NNMT (PDB 3ROD) were also used in LigPlot+³⁶ and Maestro 11 (Schrodinger LLC, New York, NY)³⁷ to analyze hydrogen bonding patterns and intermolecular interactions within 4 Å distance between residues in the NNMT substrate-binding pocket and the inhibitor analogues. The NCA substrate site in NNMT/inhibitor contact diagrams was used to describe and develop the initial SAR parameters for this system.

■ ASSOCIATED CONTENT

Supporting Information

The Supporting Information is available free of charge on the ACS Publications website at DOI: 10.1021/acs.jmedchem.7b00389.

Detailed synthesis of reaction intermediates and quinoline/isoquinoline precursors; ¹H NMR spectra of analogues synthesized in house and reaction intermediates; table of analogues purchased from commercial vendors; table of IC₅₀ and Vina scores for *N*-methyl analogues (PDF)

Molecular formula strings (CSV)

■ AUTHOR INFORMATION

Corresponding Author

*Phone: (409) 747-4749. Fax: (409) 747-4745. Email: watowich@xray.utmb.edu.

ORCID

Stanley J. Watowich: 0000-0002-1660-1818

Author Contributions

All authors contributed in a significant way to the manuscript. H.N. conducted experiments, data analysis, and interpretation, prepared the manuscript, and participated in the conceptualization of the project and design of analogues. H.L.W. participated in the design of analogues, synthesized all analogues reported in the manuscript, and wrote/edited the manuscript. V.V. conducted biochemical assays and performed IC₅₀ calculations. J.D.H., S.F.M., and S.J.W. conceptualized the project, designed analogues, analyzed and interpreted data, and edited the manuscript. All authors have read and approved the final manuscript.

Notes

The authors declare no competing financial interest.

ACKNOWLEDGMENTS

We thank Drs. C. Finnerty and C. Porter for helpful discussions. This work was supported by Department of Defense Peer Reviewed Medical Research Program grant PR141776 (S.J.W.) and a University of Texas Medical Branch Technology Commercialization Award (S.J.W.).

ABBREVIATIONS USED

NNMT, nicotinamide-*N*-methyltransferase; SAR, structure–activity relationship; SAM, *S*-(*S*'-adenosyl)-*L*-methionine; NCA, nicotinamide; 1-MNA, 1-methylnicotinamide; SAH, *S*-*S*'-adenosylhomocysteine; 1-MQ, 1-methylquinolinium; hNNMT, human nicotinamide-*N*-methyltransferase; hPNMT, human phenylethanolamine-*N*-methyltransferase; IPTG, isopropyl- β -D-1-thiogalactopyranoside; IPA, 2-propanol; MeOTf, methyl trifluoromethanesulfonate; MeI, iodomethane

REFERENCES

- (1) Alston, T. A.; Abeles, R. H. Substrate specificity of nicotinamide methyltransferase isolated from porcine liver. *Arch. Biochem. Biophys.* **1988**, *260* (2), 601–608.
- (2) Aksoy, S.; Szumlanski, C. L.; Weinshilboum, R. M. Human liver nicotinamide *N*-methyltransferase. cDNA cloning, expression, and biochemical characterization. *J. Biol. Chem.* **1994**, *269* (20), 14835–14840.
- (3) Cantoni, G. L. Methylation of nicotinamide with soluble enzyme system from rat liver. *J. Biol. Chem.* **1951**, *189* (1), 203–216.
- (4) Rini, J.; Szumlanski, C.; Guercioli, R.; Weinshilboum, R. M. Human liver nicotinamide *N*-methyltransferase: ion-pairing radiochemical assay, biochemical properties and individual variation. *Clin. Chim. Acta* **1990**, *186* (3), 359–374.
- (5) Yan, L.; Otterness, D. M.; Craddock, T. L.; Weinshilboum, R. M. Mouse liver nicotinamide *N*-methyltransferase: cDNA cloning, expression, and nucleotide sequence polymorphisms. *Biochem. Pharmacol.* **1997**, *54* (10), 1139–1149.
- (6) Riederer, M.; Erwa, W.; Zimmermann, R.; Frank, S.; Zechner, R. Adipose tissue as a source of nicotinamide *N*-methyltransferase and homocysteine. *Atherosclerosis* **2009**, *204* (2), 412–417.
- (7) Xu, J.; Moatamed, F.; Caldwell, J. S.; Walker, J. R.; Kraiem, Z.; Taki, K.; Brent, G. A.; Hershman, J. M. Enhanced expression of nicotinamide *N*-methyltransferase in human papillary thyroid carcinoma cells. *J. Clin. Endocrinol. Metab.* **2003**, *88* (10), 4990–4996.
- (8) Roessler, M.; Rolling, W.; Palme, S.; Hagmann, M. L.; Berndt, P.; Engel, A. M.; Schneider, B.; Pfeffer, M.; Andres, H.; Karl, J.; Bodenmuller, H.; Ruschoff, J.; Henkel, T.; Rohr, G.; Rossol, S.; Rosch, W.; Langen, H.; Zolg, W.; Tacke, M. Identification of nicotinamide *N*-methyltransferase as a novel serum tumor marker for colorectal cancer. *Clin. Cancer Res.* **2005**, *11* (18), 6550–6557.
- (9) Sartini, D.; Muzzonigro, G.; Milanese, G.; Pierella, F.; Rossi, V.; Emanuelli, M. Identification of nicotinamide *N*-methyltransferase as a

novel tumor marker for renal clear cell carcinoma. *J. Urol.* **2006**, *176* (5), 2248–2254.

- (10) Sartini, D.; Santarelli, A.; Rossi, V.; Goteri, G.; Rubini, C.; Ciavarella, D.; Lo Muzio, L.; Emanuelli, M. Nicotinamide *N*-methyltransferase upregulation inversely correlates with lymph node metastasis in oral squamous cell carcinoma. *Mol. Med.* **2007**, *13* (7–8), 415–421.

- (11) Tomida, M.; Mikami, I.; Takeuchi, S.; Nishimura, H.; Akiyama, H. Serum levels of nicotinamide *N*-methyltransferase in patients with lung cancer. *J. Cancer Res. Clin. Oncol.* **2009**, *135* (9), 1223–1229.

- (12) Parsons, R. B.; Smith, M. L.; Williams, A. C.; Waring, R. H.; Ramsden, D. B. Expression of nicotinamide *N*-methyltransferase (E.C. 2.1.1.1) in the Parkinsonian brain. *J. Neuropathol. Exp. Neurol.* **2002**, *61* (2), 111–124.

- (13) Williams, A. C.; Ramsden, D. B. Autotoxicity, methylation and a road to the prevention of Parkinson's disease. *J. Clin. Neurosci.* **2005**, *12* (1), 6–11.

- (14) Salek, R. M.; Maguire, M. L.; Bentley, E.; Rubtsov, D. V.; Hough, T.; Cheeseman, M.; Nunez, D.; Sweatman, B. C.; Haselden, J. N.; Cox, R. D.; Connor, S. C.; Griffin, J. L. A metabolomic comparison of urinary changes in type 2 diabetes in mouse, rat, and human. *Physiol. Genomics* **2007**, *29* (2), 99–108.

- (15) Kraus, D.; Yang, Q.; Kong, D.; Banks, A. S.; Zhang, L.; Rodgers, J. T.; Pirinen, E.; Pulinilkunnil, T. C.; Gong, F.; Wang, Y. C.; Cen, Y.; Sauve, A. A.; Asara, J. M.; Peroni, O. D.; Monia, B. P.; Bhanot, S.; Alhonen, L.; Puigserver, P.; Kahn, B. B. Nicotinamide *N*-methyltransferase knockdown protects against diet-induced obesity. *Nature* **2014**, *508* (7495), 258–262.

- (16) Kannt, A.; Pfenninger, A.; Teichert, L.; Tonjes, A.; Dietrich, A.; Schon, M. R.; Kloting, N.; Bluher, M. Association of nicotinamide-*N*-methyltransferase mRNA expression in human adipose tissue and the plasma concentration of its product, 1-methylnicotinamide, with insulin resistance. *Diabetologia* **2015**, *58* (4), 799–808.

- (17) Liu, M.; Li, L.; Chu, J.; Zhu, B.; Zhang, Q.; Yin, X.; Jiang, W.; Dai, G.; Ju, W.; Wang, Z.; Yang, Q.; Fang, Z. Serum *N*(1)-methylnicotinamide is associated with obesity and diabetes in Chinese. *J. Clin. Endocrinol. Metab.* **2015**, *100* (8), 3112–3117.

- (18) Martin, J. L.; McMillan, F. M. SAM (dependent) I AM: the *S*-adenosylmethionine-dependent methyltransferase fold. *Curr. Opin. Struct. Biol.* **2002**, *12* (6), 783–793.

- (19) Syed, S. K.; Kim, S.; Paik, W. K. Comparative studies on *S*-adenosyl-*L*-methionine binding sites of protein *N*-methyltransferases, using 8-azido-*S*-adenosyl-*L*-methionine as photoaffinity probe. *J. Protein Chem.* **1993**, *12* (5), 603–612.

- (20) Copeland, R. A.; Solomon, M. E.; Richon, V. M. Protein methyltransferases as a target class for drug discovery. *Nat. Rev. Drug Discovery* **2009**, *8* (9), 724–732.

- (21) Borchardt, R. T.; Eiden, L. E.; Wu, B.; Rutledge, C. O. Sinefungin, a potent inhibitor of *S*-adenosylmethionine: protein *O*-methyltransferase. *Biochem. Biophys. Res. Commun.* **1979**, *89* (3), 919–924.

- (22) Daigle, S. R.; Olhava, E. J.; Therkelsen, C. A.; Basavapathruni, A.; Jin, L.; Boriack-Sjodin, P. A.; Allain, C. J.; Klaus, C. R.; Raimondi, A.; Scott, M. P.; Waters, N. J.; Chesworth, R.; Moyer, M. P.; Copeland, R. A.; Richon, V. M.; Pollock, R. M. Potent inhibition of DOT1L as treatment of MLL-fusion leukemia. *Blood* **2013**, *122* (6), 1017–1025.

- (23) Cai, X. C.; Kapilashrami, K.; Luo, M. Synthesis and assays of inhibitors of methyltransferases. *Methods Enzymol.* **2016**, *574*, 245–308.

- (24) Peng, Y.; Sartini, D.; Pozzi, V.; Wilk, D.; Emanuelli, M.; Yee, V. C. Structural basis of substrate recognition in human nicotinamide *N*-methyltransferase. *Biochemistry* **2011**, *50* (36), 7800–7808.

- (25) van Haren, M. J.; Sastre Torano, J.; Sartini, D.; Emanuelli, M.; Parsons, R. B.; Martin, N. I. A rapid and efficient assay for the characterization of substrates and inhibitors of nicotinamide *N*-methyltransferase. *Biochemistry* **2016**, *55* (37), 5307–5315.

- (26) Patel, M.; Vasaya, M. M.; Asker, D.; Parsons, R. B. HPLC-UV method for measuring nicotinamide *N*-methyltransferase activity in

biological samples: evidence for substrate inhibition kinetics. *J. Chromatogr. B: Anal. Technol. Biomed. Life Sci.* **2013**, *921–922*, 87–95.

(27) Bissantz, C.; Kuhn, B.; Stahl, M. A medicinal chemist's guide to molecular interactions. *J. Med. Chem.* **2010**, *53* (14), 5061–5084.

(28) Muller, K.; Faeh, C.; Diederich, F. Fluorine in pharmaceuticals: looking beyond intuition. *Science* **2007**, *317* (5846), 1881–1886.

(29) Cowan-Jacob, S. W.; Fendrich, G.; Floersheimer, A.; Furet, P.; Liebetanz, J.; Rummel, G.; Rheinberger, P.; Centeleghe, M.; Fabbro, D.; Manley, P. W. Structural biology contributions to the discovery of drugs to treat chronic myelogenous leukaemia. *Acta Crystallogr., Sect. D: Biol. Crystallogr.* **2007**, *63* (1), 80–93.

(30) Hann, M. M.; Keseru, G. M. Finding the sweet spot: the role of nature and nurture in medicinal chemistry. *Nat. Rev. Drug Discovery* **2012**, *11* (5), 355–365.

(31) Yang, W.; Li, L.; Wang, Y.; Wu, X.; Li, T.; Yang, N.; Su, M.; Sheng, L.; Zheng, M.; Zang, Y.; Li, J.; Liu, H. Design, synthesis and biological evaluation of isoquinoline-based derivatives as novel histone deacetylase inhibitors. *Bioorg. Med. Chem.* **2015**, *23* (17), 5881–5890.

(32) Nishikawa-Shimono, R.; Sekiguchi, Y.; Koami, T.; Kawamura, M.; Wakasugi, D.; Watanabe, K.; Wakahara, S.; Kimura, K.; Yamanobe, S.; Takayama, T. Isoquinoline derivatives as potent CRTH2 antagonists: design, synthesis and SAR. *Bioorg. Med. Chem.* **2013**, *21* (24), 7674–7685.

(33) Neelakantan, H.; Vance, V.; Wang, H. L.; McHardy, S. F.; Watowich, S. J. Noncoupled fluorescent assay for direct real-time monitoring of nicotinamide N-methyltransferase activity. *Biochemistry* **2017**, *56* (6), 824–832.

(34) Viswanathan, U.; Tomlinson, S. M.; Fonner, J. M.; Mock, S. A.; Watowich, S. J. Identification of a novel inhibitor of dengue virus protease through use of a virtual screening drug discovery Web portal. *J. Chem. Inf. Model.* **2014**, *54* (10), 2816–2825.

(35) Trott, O.; Olson, A. J. AutoDock Vina: improving the speed and accuracy of docking with a new scoring function, efficient optimization, and multithreading. *J. Comput. Chem.* **2010**, *31* (2), 455–461.

(36) Wallace, A. C.; Laskowski, R. A.; Thornton, J. M. LIGPLOT: a program to generate schematic diagrams of protein-ligand interactions. *Protein Eng., Des. Sel.* **1995**, *8* (2), 127–134.

(37) *Schrödinger Release 2017-1: Maestro*; Schrödinger, LLC: New York, 2017.